A Bi-Directional Distributed Multi-User MIMO Testbed Using Digital Sigma-Delta-Over-Fiber

Achim Vandierendonck, Kang-Lun Chiu, Caro Meysmans, Fatemeh Zardosht, Xin Wang, Haolin Li, Piet Demeester *Fellow, IEEE*, and Guy Torfs, *Senior Member, IEEE*

***Abstract*—Sigma-Delta modulated signals over fiber is proposed for fronthauling of distributed signals. Analog Radio-over-Fiber (ARoF) provides perfect synchronization, but linearity is directly impacted by the required circuit elements. Digital Radio-over-Fiber (DRoF) has a low cost of implementation but complicates synchronization. Sigma-Delta modulated signals over fiber combines the synchronization benefit from ARoF and the low cost of DRoF. In this work, we show a simplified and synchronous distributed multiple-input multiple-output (MIMO) communication system for both up-link and down-link transmission, based on our real-time sigma-delta modulated signals over fiber front-haul network. The testbed uses a carrier frequency of 3.686 GHz and is composed of 4 distributed units with 4 antennas each, totaling 16 antennas. The received clock is used to provide synchronization between the central and distributed units. With this implementation, we demonstrate distributed multi-user MIMO. The synchronicity of the system is demonstrated by performing over-the-air channel reciprocity calibration and reciprocity-based uplink transmission. This is verified using 64-QAM OFDM symbols. Measurement results for 2 users / 4 users show an average error vector magnitude for up-link of 2.51% (-32.02 dB) / 2.89% (-30.79 dB) and for down-link of 4.23% (-27.48 dB) / 6.09% (-24.31 dB) respectively.**

***Index Terms*—6G, Distributed MIMO, Cell-free MIMO, ΣΔ-RoF, SDoF, DRoF.**

I. Introduction

WIRELESS data rates have doubled every eighteen months over the past few decades, as predicted by Edholm's law [1]. According to ITU-R 2020/beyond, there are three main types of scenarios: (1) enhanced mobile broadband, (2) massive machine type communication, and (3) ultra reliable and low latency communication. Different use cases, along with the current and future trends, will result in a great diversity/variety of requirements [2]. In the sixth-generation mobile networks (6G), the link capability is expected to improve by at least a factor of ten compared to the fifth-generation (5G) [3]. Densifying networks is one of the primary ways to provide high per-user data rates [4]. This can be achieved by increasing spectral efficiency using large antenna arrays to strive for more spatial diversity [5]. As the cellular networks currently stand, the majority of the antenna deployments will be carried out for sub-6GHz bands. However, such large arrays increase the total physical aperture of the radiating elements.

From another point of view, in a conventional cellular network, each User Equipment (UE) is connected to only one Access Point (AP) within each cell. At a given time instance, these APs receive different numbers of active UEs' signals, causing inter-cell interference. In order to mitigate this interference and have a more uniform quality of service and throughput, cooperation between APs such as Coordinated Multi-Point (CoMP) processing becomes a promising solution [6], [7]. CoMP has also been adopted in 3rd Generation Partnership Project (3GPP) Long Term Evolution Advanced (LTE-A) as a scheme to improve coverage, cell-edge throughput, and system efficiency [8]. However, original network-centric CoMP systems are equivalent to deploying a larger conventional cellular network with distributed antennas in each cell as interpreted in [9]. Conversely, when co-processing is implemented in a user-centric fashion, each user is served by coherent joint transmission from its selected subset of APs (user-specific cluster), while all the APs that affect the user take its interference into consideration. Hence, this approach eliminates the cell boundaries resulting in no inter-cell interference. Distributed MIMO (D-MIMO) (or Cell-free MIMO) is used to enlarge user coverage and improve the quality of edge users, with respect to current centralized cellular architectures [10].

To enable cell-free Distributed Massive MIMO (D-MaMIMO), we expect the fronthaul network to have high capacity, high scalability, low latency, and low deployment cost. Most importantly, the network should provide precise synchronization between different remote units in both time and frequency [11]. Radio-over-Fiber (RoF) technology is one of the most convincing candidates for the fronthaul network owing to its high capacity and low loss [12]. The Sigma-Delta modulated signals over Fiber (SDoF) technique has been proposed in [13] as an implementation of RoF that preserves synchronization while allowing maximal reuse of existing

A. Vandierendonck, C. Meysmans, F. Zardosht, X. Wang, P. Demeester and G. Torfs are with IDLab, Department of Information Technology, Ghent University-imec, B-9052 Ghent, Belgium (e-mail: achim.vandierendonck@ugent.be; fatemeh.zardosht@ugent.be; caro.meysmans@ugent.be; xin.wang@ugent.be; piet.demeester@ugent.be; guy.torfs@ugent.be).

H. Li was with IDLab during this work, but is now with iCana, B-3000 Leuven, Belgium.

K.-L. Chiu was with the Institute of Electronics, National Yang Ming Chiao Tung University, Hsinchu 30010, Taiwan, but is now with MediaTek Inc., Hsinchu Science Park, Hsinchu City 300, Taiwan.

This work was supported by the ERC Advanced Grant ATTO (No. 695495), ERC-POC DCAP (No. 101158037), EU H2020 ERC-POC BI-SDMoF (No. 839200), EU H2020 Int5Gent (No. 957403) project, and Research Foundation Flanders (FWO) under Grant SB (3S043919), ORINoCO (G0D7519N) and SMART-STRIP (S006224N).

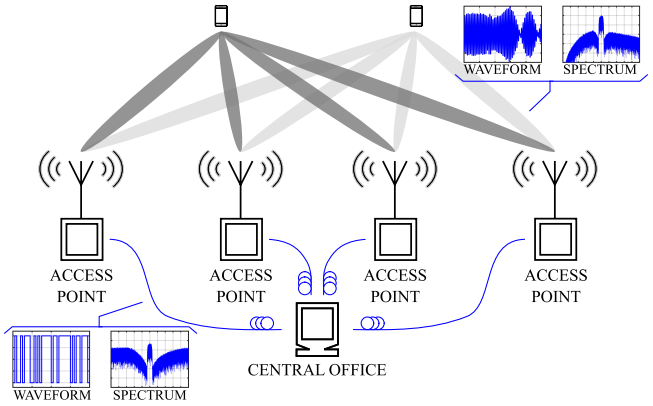

Fig. 1. Distributed Multi-User MIMO system architecture using Sigma-Delta modulated signal over fiber between the central office and the access points.

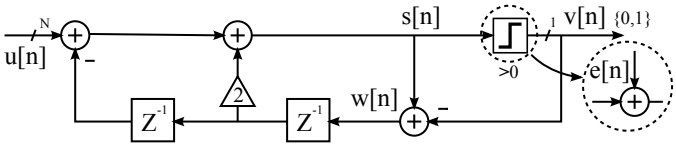

Fig. 2. Block diagram of a regular single-loop second-order low-pass sigma-delta modulator with a two-level quantizer.

hardware. Several works on developing SDoF systems from our group have already been reported in [14]–[19].

This paper is an invited extension of our work presented at OFC 2024 [20], extended with up-link measurements. Section II gives an overview of SDoF architectures, focusing on the up-link implementation. A full D-MIMO down-link and up-link fronthaul architecture using clock recovery from the down-link is shown in Section III. An experiment that uses the synchronous distributed remote radio units is implemented in Section IV, showing a reciprocity based distributed MIMO transmission. In Section V, a description of our testbed is given, and the results are discussed. Lastly, Section VI concludes this paper.

II. Sigma-Delta-over-Fiber Architectures

Digital Radio-over-Fiber (DRoF) methods such as CPRI and eCPRI use a binary representation of the baseband radio signal to transport digital data through the fronthaul network (Fig. 1). Digital transmission benefits from the reuse of standard optical transceivers ensuring low-cost operation. The downside, in case of CPRI, is that the time domain I/Q baseband samples received at the Remote Radio Unit (RRU) still require de-serialization, buffering, conversion to analog signals and up-mixing, complicating synchronization between different RRUs. By modulating the radio signal directly on an optical carrier, as is the case in Analog Radio-over-Fiber (ARoF), the RRU only requires amplification, providing perfect synchronization between the RRU and Distributed Unit (DU) as all the signals are generated at the DU. In the case of analog signals being transmitted through the fronthaul network, the linearity of the optical modulators and receiver circuits directly impact the performance of the wireless link.

TABLE I
Comparison of different sigma-delta over fiber demonstrators

Ref	SDM Rate [GHz]	Baudrate [MBd]	OSR	EVM [%]	SNR [dB]	Center Frequency [GHz]	ΣΔ generation
[14]	14	87.5	80	0.87	41	3.5	Real-Time
	14	437.5	16	2.67	31	3.5	Real-Time
[18]	9.83	160.32	31	4.74	26	25*	Real-Time
	9.83	299.2	16	6.31	24	25*	Real-Time
[19]	7.37	40.96	68	2.37	32	3.68	Real-Time
[21]	5	100	25	1.25	38	1	Real-Time
	5	198	13	2.80	31	1	Real-Time
[22]	32	1000	16	5.80	25	12	Matlab
	32	500	32	4.30	27	12	Matlab
	32	250	64	3.30	30	12	Matlab
[23]	100	390.625	128	3.58	29	25	Real-Time
	100	781.25	64	5.43	25	25	Real-Time
[24]	2×50	390.625	128	3.71	29	25	Matlab
	2×60	468.75	128	4.52	27	30	Matlab
[25]	25	700	18	5.62	25	28*	Matlab
	25	500	25	2.66	32	28*	Matlab

* Requires external mixing circuit to up-convert to mmWave.

By using Sigma-Delta modulated signals over Fiber (SDoF), the low-cost transceivers can be reused to transmit analog signals, similar to DRoF. Using Sigma-Delta Modulation (SDM), a digital representation of a baseband radio signal is oversampled, quantized and can (optionally) be modulated on an RF carrier. In the case of a 1-bit SDM, a two-level quantizer is used, resulting in a digital bit-stream. A representation of the modulator is shown in Fig. 2. An N-bit signal $\mathrm{u[n]}$ is quantized to a 1-bit signal $\mathrm{v[n]}$, however, this quantization will add significant noise, represented by $\mathrm{e[n]}$ in the block diagram. Feedback is added around the quantizer by extracting

$$\begin{aligned} w[n] &= s[n] - v[n] \\ &= s[n] - (s[n] + e[n]) \\ &= -e[n] \end{aligned} \tag{1}$$

and shaping it in such a way that it is pushed outside the band of interest. The higher the modulator sampling frequency with respect to the the multi-level baseband signal, the less quantization noise will be added in the frequency band where the baseband signal resided. The resulting bit-stream can now be transported over the existing fronthaul network and is robust against any non-linearity in the analog interfaces. As the analog signal can be recovered using only a band-pass filter, the process is fully transparent and preserves the synchronization between the DU and RRU, similar to ARoF. In Fig. 1 the SDM signals are used to transport signals between the central office and the Access Points (APs) over optical fiber. The limitations of SDoF are the Oversampling Ratio (OSR) and the order of the feedback filter. To achieve high SNR, a higher order modulator is required which has more noise suppression at lower frequencies where the baseband signal resided, but higher order modulators become complex to implement, and they are more prone to instability due to the higher number of integrators required. Another way is to increase the OSR with respect to the signal bandwidth, but reaching higher sampling speed requires more advanced technologies and limits the reuse of existing infrastructure.

Table I summarizes different SDoF demonstrations found in literature. In [14], two parallel second order SDMs with

a SDM rate of 14 GHz are implemented to modulate a 437.5 MBd (875 MHz bandwidth) signal, resulting in an OSR of 16. The resulting signals were digitally upconverted to 3.5 GHz. This modulator could theoretically reach 40 dB of in-band quantization noise suppression [26], but performance was limited by thermal noise in the driver and receiver circuits, and jitter in the transmitter circuit. In order to push the data rates higher than the chromatic dispersion limit, the implementation of [24] uses I/Q baseband samples at 28 GS/s together with a 2:1 multiplexer IC to drive parallel Electro-Absorption Modulators (EAMs) to generate a 112 GS/s bit-stream used for transmitting 437.5 MBd around a 28 GHz RF carrier frequency. This effectively halves the sample rate and bandwidth required of the optical transceivers.

In these implementations the carrier frequency was linked to the sampling frequency of the SDM bit-stream. To decouple the SDM sampling frequency from the RF carrier frequency, the received SDoF signals in [25] are up-converted using a mixer. The oscillator used for up-conversion is no longer synchronized, but this can be solved by recovering a reference from the incoming bit-stream at the RRU using a Clock- and Data Recovery (CDR) circuit. However, the performance of the wireless link will now degrade with the quality of the oscillator, and thus the recovered reference. Jitter-cleaning using a low-bandwidth Phase Locked Loop (PLL) is demonstrated in [16] and extended in [19] by extracting the reference from an interleaved bit-stream and transmitting the resampled, selected stream at different RRUs. Comparing this topology to DRoF, only a single bit digital to analog converter is required in the RRU.

III. Sigma-Delta Modulation based Distributed MIMO Testbed

A. Previous work

All above implementations focus on the down-link transmission from the Central Unit (CU) to the User Equipment (UE). In order to implement the up-link transmission, the received RF data at the Remote Radio Unit (RRU) from the user needs to be sent through the fronthaul network back to the CU. In [27] a triangle wave is embedded in a Sigma-Delta modulated signals over Fiber (SDoF) stream during receive and used in the RRU to modulate the received RF signal. Frequency down-conversion is performed at the CU, eliminating the requirement for oscillators and mixers, keeping the processing required at the RRU low. As this approach embeds the analog signal in a binary datastream, much like the Sigma-Delta Modulation (SDM) down-link signals, this realizes a synchronous return path to enable coherent spatial processing. Using this topology the authors measured an Error Vector Magnitude (EVM) of $5.2\,\%$ and $6.9\,\%$ for two UEs and three RRUs while transmitting 5 MBd 16QAM signals.

Fig. 3 shows the SDoF based Multi-User MIMO (MU-MIMO) demonstration based on our preceding 4×2 work [16]. A computer serves as the CU and communicates with the DU over the PCIe interface. The DU (Fig. 4a) is a Field Programmable Gate Array (FPGA) that receives the I/Q samples from the CU and converts them to antenna streams using

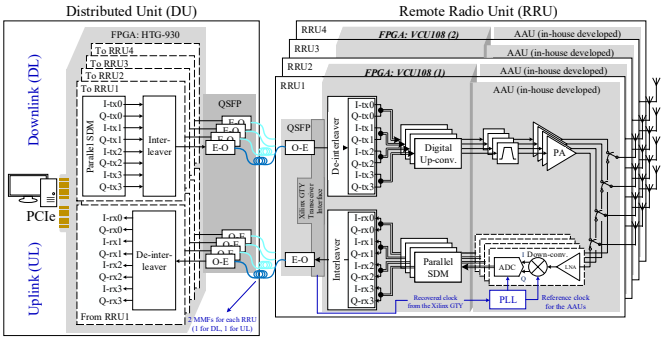

Fig. 3. Testbed system architecture with a single DU connected to four RRUs using fiber.

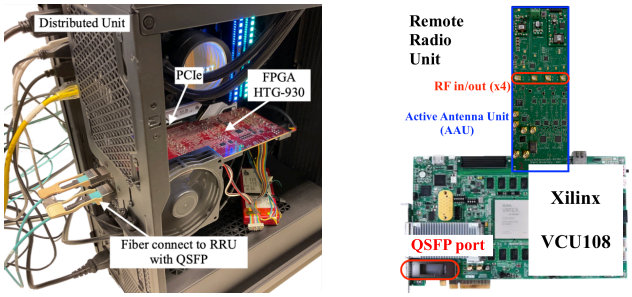

(a) DU (b) RRU

Fig. 4. Testbed components

SDM. These individual streams are bit-interleaved and sent via the QSFP interface over optical fiber to the RRU (Fig. 4b). Each of the RRUs is also an FPGA connected to the DU by two 28 Gbps multi-mode fiber links, one is used for the up-link data path and another for the down-link. The RRUs have four antennas that can serve as Access Points (APs) when they are configured as transmitters. They de-interleave the data from the QSFP interface and send specific streams to each of their antennas. Each antenna stream is first digitally up-converted and finally filtered and amplified on a custom designed module. Each of RRUs can serve four antennas using Time Division Duplexing (TDD) in either transmit or receive direction. TDD was chosen to be compatible with the 5G standard in the 3.5 GHz band. It also reduces the hardware complexity as it foregoes the need for a diplexing filter. Using TDD, we ensure that the channel is the same in both up-link and down-link transmission, this overcomes the need for channel feedback.

The RRU hardware can also be reused for the UEs when they are configured as receivers. In that scenario the received RF signal is amplifier and down-converted before it is digitized and processed on the FPGA. The RRU modulates each antenna stream using SDM before interleaving them to be sent back to the DU. On the DU the received interleaved data is de-interleaved and filtered before they are made available to the CU using the PCIe interface. A single RRU is equivalent to four, single-stream, UEs. In the setup, four RRUs are configured as distributed APs and one RRU is used to demonstrate a four user scenario. A breakdown of the utilization for the DU and RRU is shown in Table II.

TABLE II
FPGA RESOURCE UTILIZATION

Resource	DU	RRU
LUT	212876	337401
LUTRAM	28085	39066
FF	287613	378764
BRAM	510	366.5
DSP	627	131
IO	16	274
GT	24	12
BUFG	23	28
MMCM	1	3
PLL	1	3

TABLE III
SIGNAL PARAMETERS

Carrier frequency (f_c)	3.6864 GHz
Data bandwidth	46.08 MHz
Subcarrier spacing	360 kHz
Cyclic prefix (CP) size	0.69 μs (0.25×)
FFT size	128 points
DC + Null subcarrier	14 points
Pilot subcarrier	10 points
Data rate (64-QAM)	180 Mbps/user

B. Down-Link

Table III shows the signal parameters associated with our setup. During down-link transmission, baseband I/Q samples are generated in the DU which is composed of a dedicated computer. Using a PCIe interface, these samples are sent to the memory of an FPGA board and modulated using a parallel SDM to a 1-bit signal. The four SDM streams for a single RRU are encapsulated in a single datastream and are sent via the optical link using the FPGA Quad Small Form-factor Pluggable (QSFP28) transceivers. At the RRU the datastream is decomposed into the four sigma-delta modulated streams, one for each antenna. Employing the same method used in [19], the I/Q samples are digitally upconverted to the carrier frequency of 3.6864 GHz. The recovered clock from the datastream is cleaned using low-bandwidth Phase Locked Loops (PLLs) and available for external up-mixing and/or the up-link path. To ensure that the radio signals from different APs correctly interfere at the users, phase synchronization between different RRUs is very important [28]. The use of the recovered clock ensures phase stability between the RRUs. In comparison to Digital Radio-over-Fiber (DRoF), a simple 1-bit Digital to Analog Converter (DAC) is required, which combined with a band-pass filter, reconstructs the analog waveform. Final amplification is done before the RF signal is transmitted. Similar to Analog Radio-over-Fiber (ARoF), this link is fully transparent and synchronous from the perspective of the DU, this allows channel compensation to be applied at the DU, keeping the required processing on the RRU low.

C. Up-Link

The UE transmits data wirelessly during up-link to the APs at the RRUs. Using the jitter-cleaned clock recovered from the down-link path, the incoming RF data is down-mixed and sampled by the Analog to Digital Converters (ADCs). To transmit the data through the fronthaul network back to the DU, the ADC samples are sigma-delta modulated by the FPGA. Using the same interleaving structure as the down-link, all four antenna streams are combined and sent over optical fiber. At the DU the datastream is decomposed back into the four sigma-delta modulated antenna streams after which the quantization noise is filtered out, recovering the received baseband I/Q samples. As is the case during down-link transmission, these operations are fully transparent and synchronous. The architecture used in [27] has significantly less complexity at the RRU but are limited to a fronthaul rate of 10 Gbps and report a higher EVM due to the increased jitter, which degrades the up-link signal quality.

To reduce the fronthaul bandwidth, multi-user decoding can be performed on the RRU itself before transmitting the data back to the DU. True time delay beamforming is difficult to implement in analog circuits due to the signal delays required. However, the asynchronous sigma-delta modulation shown in [29] can be used to modulate the received antenna streams into a binary representation. While not implemented in this work, this would allow analog beamforming at the RRU by delaying this binary representation using inverters and combining them using a synchronous sigma-delta modulator. This preprocessed signal can then be transmitted back to the DU.

IV. CHANNEL RECIPROCITY CALIBRATION

The testbed described in Section III is used to transmit and receive Distributed MIMO (D-MIMO) data. To make sure that the interference from all Access Points (APs) to all users are taken into account, aside from synchronization, careful calibration is required to model the channel and hardware imperfections. This section elaborates on how a channel reciprocity calibration strategy without user involvement is implemented on the testbed by using a reference antenna.

Considering a narrowband (one subcarrier) 2×2 Multiple-Input Multiple-Output (MIMO) system as proposed in [30]–[32] with circuit mismatch effects and ignoring AWGN, the up-link transmission can be formed as

$$\mathbf{y_U} = \mathbf{\Gamma_r H \Psi_t x_U} \tag{2}$$

$$\begin{bmatrix} y_1 \\ y_2 \end{bmatrix}_{\mathrm{U}} = \begin{bmatrix} \gamma_{1,\mathrm{r}} & 0 \\ 0 & \gamma_{2,\mathrm{r}} \end{bmatrix} \begin{bmatrix} h_{11} & h_{12} \\ h_{21} & h_{22} \end{bmatrix} \begin{bmatrix} \psi_{1,\mathrm{t}} & 0 \\ 0 & \psi_{2,\mathrm{t}} \end{bmatrix} \begin{bmatrix} x_1 \\ x_2 \end{bmatrix}_{\mathrm{U}}, \tag{3}$$

where $\mathbf{\Gamma}$ is the channel response associated with the Remote Radio Unit (RRU) AP receive circuit, with each channel denoted as γ; $\mathbf{H} \in \mathbb{C}^{M \times K}$ is the baseband MIMO channel matrix; $\mathbf{\Psi}$ is the response of the User Equipment (UE) transmitter circuit, with each element denoted as ψ; $\mathbf{x_U}$ and $\mathbf{y_U}$ are up-link transmit and receive signal vectors. We can further define

$$\mathbf{H_{UL}} = \mathbf{\Gamma_r H \Psi_t} = \begin{bmatrix} \gamma_{1,\mathrm{r}}\psi_{1,\mathrm{t}}h_{11} & \gamma_{1,\mathrm{r}}\psi_{2,\mathrm{t}}h_{12} \\ \gamma_{2,\mathrm{r}}\psi_{1,\mathrm{t}}h_{21} & \gamma_{2,\mathrm{r}}\psi_{2,\mathrm{t}}h_{22} \end{bmatrix}. \tag{4}$$

Similarly, the down-link transmission can be formed as

$$\mathbf{y_D} = \mathbf{H_{DL}} \mathbf{F}_{\mathbf{pre}}^{\top} \mathbf{x_D}, \tag{5}$$

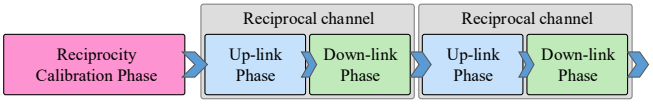

Fig. 5. System operation procedure.

where $^\top$ denotes the transpose operation, $\mathbf{F_{pre}}$ is the precoding matrix, and

$$\mathbf{H_{DL}} = \mathbf{\Psi_r} \mathbf{H}^\top \mathbf{\Gamma_t} = \begin{bmatrix} \psi_{1,\mathrm{r}}\gamma_{1,\mathrm{t}}h_{11} & \psi_{1,\mathrm{r}}\gamma_{2,\mathrm{t}}h_{21} \\ \psi_{2,\mathrm{r}}\gamma_{1,\mathrm{t}}h_{12} & \psi_{2,\mathrm{r}}\gamma_{2,\mathrm{t}}h_{22} \end{bmatrix}. \quad (6)$$

Taking Zero-Forcing (ZF) precoding $\left(\mathbf{F_{pre}} = \mathbf{H_{UL}^{-1}}\right)$ as an example,

$$\mathbf{F_{pre}} = \frac{1}{\det(\mathbf{H_{UL}})} \begin{bmatrix} \gamma_{2,\mathrm{r}}\psi_{2,\mathrm{t}}h_{22} & -\gamma_{1,\mathrm{r}}\psi_{2,\mathrm{t}}h_{12} \\ -\gamma_{2,\mathrm{r}}\psi_{1,\mathrm{t}}h_{21} & \gamma_{1,\mathrm{r}}\psi_{1,\mathrm{t}}h_{11} \end{bmatrix} \quad (7)$$

$\det(\cdot)$ is used to denote the determinant of the matrix. Eq. 5 can be expanded into

$$\begin{bmatrix} y_1 \\ y_2 \end{bmatrix}_{\mathrm{D}} = \frac{1}{\det(\mathbf{H_{UL}})} \begin{bmatrix} h_{\mathrm{eq},11} & h_{\mathrm{eq},12} \\ h_{\mathrm{eq},21} & h_{\mathrm{eq},22} \end{bmatrix} \begin{bmatrix} x_1 \\ x_2 \end{bmatrix}_{\mathrm{D}}. \quad (8)$$

where

$$h_{eq,11} = \left(\gamma_{2,r}\gamma_{1,t}h_{11}h_{22} - \gamma_{1,r}\gamma_{2,t}h_{12}h_{21}\right)\psi_{1,r}\psi_{2,t} \quad (9)$$
$$h_{eq,12} = \left(\gamma_{1,r}\gamma_{2,t} - \gamma_{2,r}\gamma_{1,t}\right)\psi_{1,r}\psi_{1,t}h_{11}h_{21} \quad (10)$$
$$h_{eq,21} = \left(\gamma_{2,r}\gamma_{1,t} - \gamma_{1,r}\gamma_{2,t}\right)\psi_{2,r}\psi_{2,t}h_{12}h_{22} \quad (11)$$
$$h_{eq,22} = \left(\gamma_{1,r}\gamma_{2,t}h_{11}h_{22} - \gamma_{2,r}\gamma_{1,t}h_{12}h_{21}\right)\psi_{2,r}\psi_{1,t} \quad (12)$$

To achieve ideal precoding,

$$\begin{bmatrix} h_{\mathrm{eq},11} & h_{\mathrm{eq},12} \\ h_{\mathrm{eq},21} & h_{\mathrm{eq},22} \end{bmatrix} = \begin{bmatrix} \det(\mathbf{H_{UL}}) & 0 \\ 0 & \det(\mathbf{H_{UL}}) \end{bmatrix}. \quad (13)$$

From the derivation, the diagonal terms can be seen as scaling factors on a UE channel and can be dealt with at the receive sides. There is no inter-user interference as long as the off-diagonal terms are zero after the calibration procedure. This is achieved if

$$\gamma_{1,\mathrm{r}}\gamma_{2,\mathrm{t}} = \gamma_{2,\mathrm{r}}\gamma_{1,\mathrm{t}}. \quad (14)$$

Without loss of generality, when the system is extended to M APs, the conditions of no interference are formed as

$$\begin{aligned} \gamma_{m,\mathrm{r}}\gamma_{n,\mathrm{t}} =& \gamma_{n,\mathrm{r}}\gamma_{m,\mathrm{t}}, \\ & \forall m, n \in M; m \neq n. \end{aligned} \quad (15)$$

Note that these conditions relate only to the AP receive and transmit circuit. In other words, the the forward paths (from n to m) and backward paths (from m to n) must be the equal for all APs.

The system operation procedure and frame structure is shown in Fig. 5. The reciprocity calibration phase operates first before any data is transmitted and is required to obtain the ratio between the up-link and down-link channel such that channel information of the up-link transmission can be reused for down-link precoding.

The authors of [33] propose an intuitively, completely distributed calibration procedure to enable implicit MIMO combining. To simplify the procedure, we set a reference antenna and assume the oscillator phase and the channel state remain stationary during forward and backward transmission.

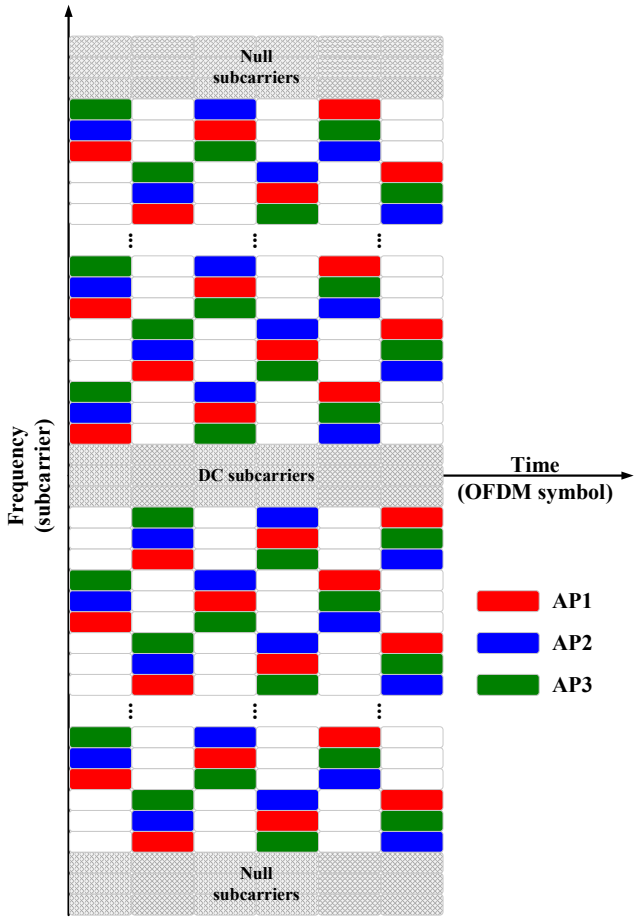

Fig. 6. Frequency interleaved training sequence

The ratio between the forward and backward transmission to this reference antenna gives the calibration coefficient:

$$h_{cc,m} = \frac{\gamma_{m,\mathrm{r}}h_{m,ref}\psi_{ref,\mathrm{t}}}{\gamma_{m,\mathrm{t}}h_{m,ref}\psi_{ref,\mathrm{r}}} \quad (16)$$

By multiplying $h_{cc,m}$ onto each DL AP path, we calibrate the mismatch between forward and backward paths, and the modified relations turns into

$$\gamma_{1,\mathrm{r}}(\gamma_{2,\mathrm{t}}h_{cc,2}) = \gamma_{1,\mathrm{r}}\gamma_{2,\mathrm{t}}\frac{\gamma_{2,\mathrm{r}}\psi_{ref,\mathrm{t}}}{\gamma_{2,\mathrm{t}}\psi_{ref,\mathrm{r}}} = \gamma_{2,\mathrm{r}}(\gamma_{1,\mathrm{t}}h_{cc,1}), \quad (17)$$

which meets the condition set by Eq. 15.

The calibration coefficients are obtained by using a training sequence inspired by [34]. We arrange the training signal into a staggered and mirror-null-ed subcarrier form as shown in Fig. 6. This sequence can accommodate at most three channels, which means that we have to divide all the antenna hardware paths into several sets as shown in Fig. 7. A reference antenna is added to the setup, this means that no user involvement is required during calibration. Frequency interleaving ensures that the phase relationship between antennas is captured and an overlapping antenna is required to obtain and compensate the phase variation along with the time difference

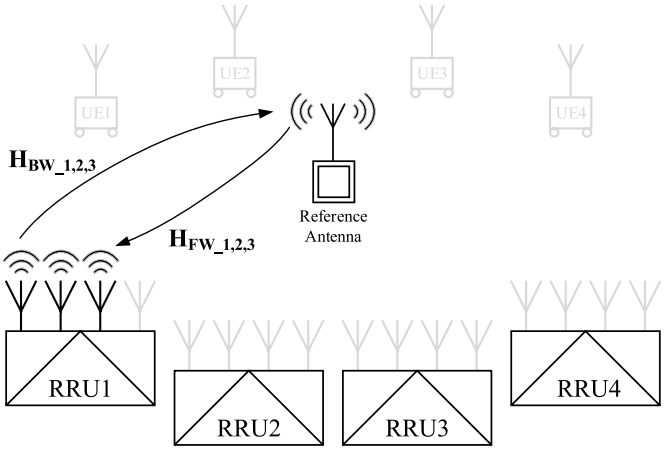

(a) Set 1: AP1,2,3

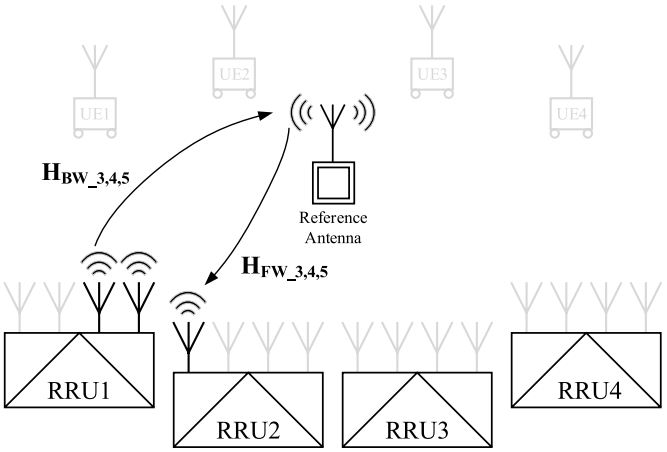

(b) Set 2: AP3,4,5

Fig. 7. The first two sets of reciprocity calibration. There is no user involvement as a reference antenna is used.

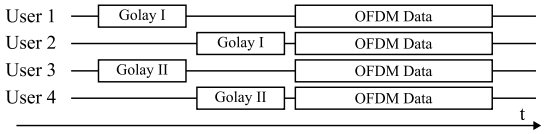

Fig. 8. Frame structure used during up-link transmission from the users to the RRUs.

among each two sets. After obtaining the coefficients of one set and the phase variation with previous, all coefficients are updated via this relation.

By utilizing the reciprocity of the wireless channel, we are able to obtain the channel coefficients directly from the UL channel estimation which can be reused for precoding the DL transmission.

After the calibration, up-link and down-link data is delivered successively through different time slots, known as Time Division Duplexing (TDD). By exploiting the reciprocity of the wireless channel, multiple access interference can be eliminated before down-link transmitting by obtaining the channel coefficients from the up-link channel estimation and reusing them in the precoding of the down-link transmission. The structure of the up-link slot is shown in Fig. 8. The

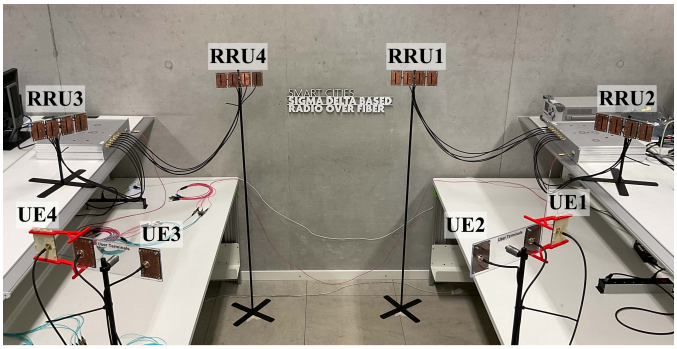

(a) Scenario photo

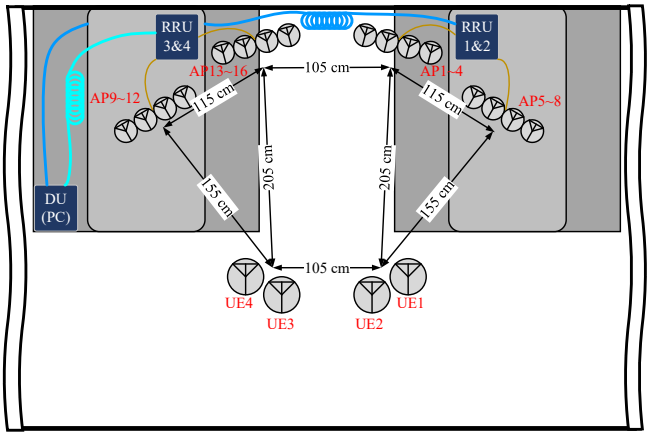

(b) Simplified layout

Fig. 9. Measurement setup

preamble is a 1280 points Golay sequence that was defined in [35] and is used to detect frame boundary and estimate the up-link temporal domain channel. Two of the user channels are estimated simultaneously using orthogonal sequence I and II. Then the other two are estimated at the next timing slot, followed by simultaneous transmission for all users. After up-link the channel information is extracted and used to pre-code the down-link data transmission. During down-link, the reciprocity calibration coefficients are combined with the channel information to simultaneously transmit preamble and OFDM data to all user.

V. Measurement Methodology and Results

The Sigma-Delta modulated signals over Fiber (SDoF) Distributed Antenna Systems (DAS) is inherently synchronous and will be used to demonstrate the reciprocity calibration, multi-user reception and reciprocity based down-link precoding. The system control signals and the physical layer digital signal processing including OFDM signal generation, MIMO detection and precoding are processed from Python scripts on the Distributed Unit (DU) PC. The measurement scenario and the simplified layout are shown in Fig. 9. The combined optical-wireless transmission performance was measured with two (one for up-link, one for down-link) 100m multi-mode fibers connecting the DU and each Remote Radio Unit (RRU). Each RRU is composed of 4 AP antennas. Each set of antennas is placed around 1m from antennas belonging to another RRU.

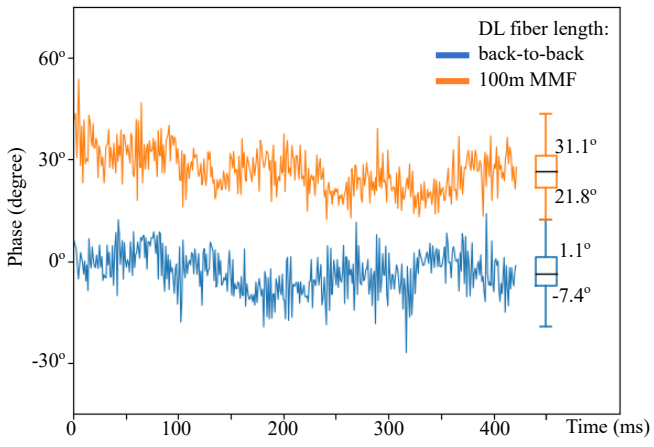

Fig. 10. RRU phase difference versus time and its distribution [19].

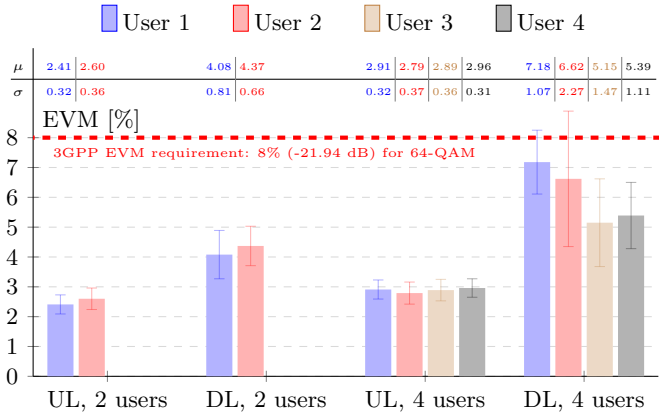

Fig. 11. Average of 50 pairs of up-link/down-link measurements.

The performance is evaluated in a two and four user scenario. After the reciprocity calibration phase, 50 up-link/down-link frames are transmitted spread over 5 minutes. For each up-link/down-link pair, two/four users first send the orthogonal Golay sequence in the different timing slot as described in Fig. 8 for estimating the MIMO channel matrix in temporal domain at the DU. This sequence is followed by 20 OFDM data symbols modulated with 64-QAM. Subsequently, the precoding matrix is calculated centrally and is combined with the calibration coefficients for generating down-link precoded training sequence and data. Each User Equipment (UE) then estimates the corresponding precoded channel along with its hardware circuit effect and demodulate the data after equalizing the residual effect.

Fig. 10 illustrated the measured RRU phase difference over time, showing that our measured Error Vector Magnitude (EVM) remains stable. Within 50 up-link/down-link pairs as shown in Fig. 11, the up-link average EVM are 2.51% (-32.02 dB) / 2.89% (-30.79 dB) and down-link average EVM are 4.23% (-27.48 dB) / 6.09% (-24.31 dB) for 64-QAM in the case of 2 users / 4 users, respectively.

VI. Conclusion

This work shows the measurement results of a practical 16×2 / 16×4 distributed Multiple-Input Multiple-Output (MIMO) Radio-over-Fiber (RoF) system implementation.

It is the first demonstration of RoF based distributed MIMO with the Access Point (AP) number up to 16 and User Equipment (UE) number up to 4. The performance and system hardware complexity while adopting a cell-free Distributed MIMO (D-MIMO) scheme are illustrated.

Making good use of the channel reciprocity, this work demonstrates how D-MIMO can be used to eliminate down-link multiple access interference by the precoding technique without heavy channel feedback. We show a clear advantage of Multi-User MIMO (MU-MIMO) by doubling the channel capacity with respect to centralized MIMO [36]. However, the non-ideality of hardware circuits which remove the reciprocity must be calibrated and compensated to obtain correct down-link signals. We have not only derived the effects but also examined the hardware calibration methods. According to the derivation, no user has to involve the calibration procedure. Reference antenna can further be removed if we properly arrange the calibration antenna combination. Furthermore, the down-link transmission performance can stay stable for more than five minutes after a single reciprocity calibration, which demonstrates the robustness and the synchronization benefits of these Sigma-Delta modulated signals over Fiber (SDoF) Distributed Antenna Systems (DAS) [37].

This testbed architecture has the benefit of being scalable for more Remote Radio Units (RRUs) and UEs. In order to reduce the fronthaul bandwidth required, future work could send the MIMO beamforming coefficients over the control channel in the datastream, which allows MIMO precoding for each antenna to be performed at the RRU. During up-link, MIMO decoding can be performed at the RRU, reducing the fronthaul bandwidth requirement.

References

[1] S. Amakawa *et al.*, "White Paper on RF enabling 6G–opportunities and challenges from technology to spectrum," University of Oulu, Tech. Rep. 13, 2021. [Online]. Available: https://www.oulu.fi/6gflagship/6g-white-paper-rf-spectrum

[2] *IMT Vision–Framework and overall objectives of the future development of IMT for 2020 and beyond*, ITU-R Std. M.2083, 2015. [Online]. Available: https://www.itu.int/dms_pubrec/itu-r/rec/m/R-REC-M.2083-0-201509-I!!PDF-E.pdf

[3] I. F. Akyildiz, A. Kak, and S. Nie, "6G and Beyond: The Future of Wireless Communications Systems," *IEEE Access*, vol. 8, pp. 133 995–134 030, 2020.

[4] J. G. Andrews *et al.*, "Are we approaching the fundamental limits of wireless network densification?" *IEEE Communications Magazine*, vol. 54, no. 10, pp. 184–190, Oct. 2016.

[5] E. G. Larsson *et al.*, "Massive MIMO for Next Generation Wireless Systems," *IEEE Communications Magazine*, vol. 52, no. 2, pp. 186–195, Feb. 2014.

[6] D. Lee *et al.*, "Coordinated multipoint transmission and reception in LTE-advanced: deployment scenarios and operational challenges," *IEEE Communications Magazine*, vol. 50, no. 2, pp. 148–155, Feb. 2012.

[7] D. N. Nguyen and M. Krunz, "Cooperative MIMO in wireless networks: recent developments and challenges," *IEEE Network*, vol. 27, no. 4, pp. 48–54, 2013.

[8] *Coordinated multi-point operation for LTE physical layer aspects*, 3GPP Std. TR 36.819, v11.0.0, Sep. 2011. [Online]. Available: https://www.3gpp.org/ftp/Specs/archive/36_series/36.819/36819-b00.zip

[9] G. Interdonato *et al.*, "Ubiquitous Cell-Free Massive MIMO Communications," *EURASIP Journal on Wireless Communications and Networking*, vol. 2019, no. 1, Aug. 2019.

[10] J. Wang and L. Dai, "Asymptotic Rate Analysis of Downlink Multi-User Systems With Co-Located and Distributed Antennas," *IEEE Transactions on Wireless Communications*, vol. 14, no. 6, pp. 3046–3058, Jun. 2015.

[11] J. Zhang *et al.*, "Cell-Free Massive MIMO: A New Next-Generation Paradigm," *IEEE Access*, vol. 7, pp. 99 878–99 888, 2019.

[12] C. Ranaweera *et al.*, "5G C-RAN With Optical Fronthaul: An Analysis From a Deployment Perspective," *Journal of Lightwave Technology*, vol. 36, no. 11, pp. 2059–2068, Jun. 2018.

[13] L. Breyne *et al.*, "Comparison Between Analog Radio-Over-Fiber and Sigma Delta Modulated Radio-Over-Fiber," *IEEE Photonics Technology Letters*, vol. 29, no. 21, pp. 1808–1811, Nov. 2017.

[14] C.-Y. Wu *et al.*, "Real-Time 4x3.5 Gbps Sigma Delta Radio-over-Fiber for a Low-Cost 5G C-RAN Downlink," in *2018 European Conference on Optical Communication (ECOC)*. IEEE, Sep. 2018.

[15] C.-Y. Wu *et al.*, "Distributed MU-MIMO Demonstration using FPGA-based Sigma-Delta-over-Fiber," in *45th European Conference on Optical Communication (ECOC 2019)*. Institution of Engineering and Technology, 2019.

[16] C.-Y. Wu *et al.*, "Demonstration of a Scalable Distributed Antenna System Using Real-Time Bit-Interleaved Sigma-Delta-Over-Fiber Architectures," in *2020 European Conference on Optical Communications (ECOC)*. IEEE, Dec. 2020.

[17] C.-Y. Wu *et al.*, "Distributed Multi-User MIMO Transmission Using Real-Time Sigma-Delta-Over-Fiber for Next Generation Fronthaul Interface," *Journal of Lightwave Technology*, vol. 38, no. 4, pp. 705–713, Feb. 2020.

[18] C.-Y. Wu *et al.*, "Distributed Antenna System Using Sigma-Delta Intermediate-Frequency-Over-Fiber for Frequency Bands Above 24 GHz," *Journal of Lightwave Technology*, vol. 38, no. 10, pp. 2765–2773, May 2020.

[19] C.-Y. Wu *et al.*, "A Bit-Interleaved Sigma-Delta-Over-Fiber Fronthaul Network for Frequency-Synchronous Distributed Antenna Systems," *Applied Sciences*, vol. 11, no. 23, p. 11471, Dec. 2021.

[20] G. Torfs *et al.*, "Sigma-Delta-over-Fiber," in *Optical Fiber Communication Conference (OFC) 2024*, ser. OFC. Optica Publishing Group, 2024, pp. 1–3.

[21] J. Wang *et al.*, "Delta-Sigma Modulation for Next Generation Fronthaul Interface," *Journal of Lightwave Technology*, vol. 37, no. 12, pp. 2838–2850, Jun. 2019.

[22] I. C. Sezgin *et al.*, "A Flexible Multi-Gbps Transmitter Using Ultra-High Speed Sigma- Delta-over- Fiber," in *2018 IEEE/MTT-S International Microwave Symposium - IMS*. IEEE, Jun. 2018.

[23] H. Li *et al.*, "Real-Time 100-GS/s Sigma-Delta Modulator for All-Digital Radio-Over-Fiber Transmission," *Journal of Lightwave Technology*, vol. 38, no. 2, pp. 386–393, Jan. 2020.

[24] J. Declercq *et al.*, "Low Power All-Digital Radio-Over-Fiber Transmission for 28-GHz Band Using Parallel Electro-Absorption Modulators," *Journal of Lightwave Technology*, vol. 39, no. 4, pp. 1125–1131, Feb. 2021.

[25] H. Bao, F. Ponzini, and C. Fager, "Flexible mm-Wave Sigma-Delta-over-Fiber MIMO Link," *Journal of Lightwave Technology*, vol. 41, no. 14, pp. 4734–4742, Jul. 2023.

[26] R. Schreier, S. Pavan, and G. C. Temes, *Understanding Delta-Sigma Data Converters*. Wiley, Mar. 2017.

[27] L. Aabel *et al.*, "A TDD Distributed MIMO Testbed Using a 1-bit Radio-Over-Fiber Fronthaul Architecture," *IEEE Transactions on Microwave Theory and Techniques*, pp. 1–13, 2024.

[28] C.-M. Chen *et al.*, "Distributed Massive MIMO: A Diversity Combining Method for TDD Reciprocity Calibration," in *GLOBECOM 2017 - 2017 IEEE Global Communications Conference*. IEEE, Dec. 2017.

[29] C. Meysmans *et al.*, "A Multi-GHz Inverter-Based ASDM With Distortion Cancellation," *IEEE Transactions on Circuits and Systems II: Express Briefs*, pp. 1–1, 2024.

[30] W.-H. Hsiao and C.-C. Huang, "A novel 5G TDD cellular system proposal based on multipath division multiple access," in *2017 19th International Conference on Advanced Communication Technology (ICACT)*. IEEE, 2017.

[31] W.-H. Hsiao, Y.-W. Shih, and C.-C. Huang, "Case study and performance evaluation of MDMA–A non-orthogonal multiple access scheme for 5G cellular systems," *Mobile Networks and Applications*, vol. 23, no. 4, pp. 1035–1048, Oct. 2017.

[32] S.-Y. Wang *et al.*, "Multipath Division Multiple Access for High Capacity 5G Millimeter Wave Cellular Systems," in *2020 IEEE Globecom Workshops*. IEEE, Dec. 2020.

[33] C. Shepard *et al.*, "Argos: practical many-antenna base stations," in *Proceedings of the 18th annual international conference on Mobile computing and networking*, ser. Mobicom'12. ACM, Aug. 2012.

[34] A. Tarighat, R. Bagheri, and A. Sayed, "Compensation schemes and performance analysis of IQ imbalances in OFDM receivers," *IEEE Transactions on Signal Processing*, vol. 53, no. 8, pp. 3257–3268, Aug. 2005.

[35] *IEEE Standard for Information Technology–Telecommunications and Information Exchange between Systems Local and Metropolitan Area Networks–Specific Requirements Part 11: Wireless LAN Medium Access Control (MAC) and Physical Layer (PHY) Specifications Amendment 2: Enhanced Throughput for Operation in License-exempt Bands above 45 GHz*, Std., 2021.

[36] C. Fager *et al.*, "Comparison of Co-located and Distributed MIMO for Indoor Wireless Communication," in *2022 IEEE Radio and Wireless Symposium (RWS)*. IEEE, Jan. 2022.

[37] H. Tataria *et al.*, "6G Wireless Systems: Vision, Requirements, Challenges, Insights, and Opportunities," *Proceedings of the IEEE*, vol. 109, no. 7, pp. 1166–1199, Jul. 2021.

Achim Vandierendonck received the M.S. degree in electrical engineering from Ghent University, Ghent, Belgium in 2019. He is currently pursuing the Ph.D. degree at the Department of Information Technology, UGent. As part of the IDLab design group, he has designed and helped designing numerous chips related to high-speed analog and digital communication. His research interests include high-speed mixed-signal designs, digital circuit design, and clock and data recovery systems.

Kang-Lun Chiu received the B.S. degree and Ph.D. degree in electrical engineering from National Dong Hwa University, Hualien City, Taiwan, in 2015 and 2023 respectively. Since 2023 he works at MediaTek Inc., Hsinchu Science Park, Hsinchu City 300, Taiwan. His research interests include digital wireless communication systems, digital signal processing, and digital VLSI systems design.

Caro Meysmans received the M.S. degree in electrical engineering from Ghent University, Ghent, Belgium in 2020. He is currently pursuing the Ph.D. degree at the Department of Information Technology, UGent. His research interests include analog circuit design, with a focus on time-domain processing and analog-to-digital converters, as well as digital circuit design.

Fatemeh (Pardise) Zardosht received the M.S. degree in electrical engineering from Shiraz University, Shiraz, Iran in 2017. She is currently pursuing the Ph.D. degree at the Department of Information Technology, UGent. Her research interests include digital and FPGA design for radio-over-fiber wireless systems, and signal processing.

Xin Wang (Student Member, IEEE) received the B.E. degree in electronic information science and technology from University of Science and Technology of China, Hefei, China, in 2010, and M.S. degree in microelectronics and solid-state electronics from Fudan University, Shanghai, China, in 2013. He is currently working towards Ph.D. degree in Ghent University, Ghent, Belgium. His research focuses on high-speed mixed-signal integrated circuit design for (opto-)electronic communication systems.

Haolin Li received the M.S. degree and Ph.D. degree in electrical engineering from Ghent University, Ghent, Belgium, in 2014 and 2019, respectively. From 2019 to 2022, he has been with Ghent University and imec as a postdoctoral researcher. Since 2022 he works at iCana in Leuven, Belgium. His research interests include signal processing, radio-over-fiber fiber-wireless systems, and digital circuit design.

Piet Demeester (Fellow, IEEE) is currently a Professor with Ghent University, Ghent, Belgium, and the Director of the IDLab, imec Research Group, UGent. The IDLab's research activities include distributed intelligence in the IoT, machine learning and data mining, semantic intelligence, cloud and big data infrastructures, fixed and wireless networking, electromagnetics, and high-frequency circuit design. He holds the Advanced ERC Grant.

Guy Torfs (Senior Member, IEEE) received the Engineering degree in applied electronics and the Ph.D. degree in applied sciences and electronics from Ghent University, Ghent, Belgium, in 2007 and 2012 respectively. Since 2011, he has been with IMEC, associated with Ghent University, where he first became part-time Assistant Professor in 2015. In 2018, he became full-time Associate Professor at Ghent University.

His research interests include high-speed mixed-signal designs for wireless, fiber-optic and backplane communication systems, including digital signal processing and calibration, analog equalization circuits, radio-over-fiber transceivers, and clock and data recovery systems.

In 2014, as part of the Bi-PON and Cascaded Bi-PON team, he was a recipient of the Greentouch 1000x award. He was a co-recipient of a 2015 DesignCon Best Paper Award in the High-Speed Signal Design category and the 2019 ECOC Best Demo Award. He has served as associate editor for IEICE Electronics Express and IEEE Transactions on Circuits and Systems-II, was member of the European conference on optical communication (ECOC) TPC and is current member of the IEEE International Solid-State Circuit Conference (ISSCC) TPC.